REPORT DOCUMENTATION PAGE

AFRL-SR-BL-TR-98-

0478

88

1. AGENCY USE ONLY *(Leave blank)*	2. REPORT DATE	3. REPORT TYPE AND DATES COVERED
	29 May 98	Final Technical Report 15 Oct 93 to 31 Dec 97

4. TITLE AND SUBTITLE
CONFORMABLE M3 MICROSYSTEMS FOR AERODYNAMIC CONTROL

5. FUNDING NUMBERS
F49620-94-1-0008

6. AUTHOR(S)
Chih-Ming Ho
Yu-Chong Tai

7. PERFORMING ORGANIZATION NAME(S) AND ADDRESS(ES)
Mechanical & Aerospace Engineering Dept
University of California, LA
Los Angeles, CA 90095

8. PERFORMING ORGANIZATION REPORT NUMBER

9. SPONSORING/MONITORING AGENCY NAME(S) AND ADDRESS(ES)
AFOSR/NA
110 Duncan Avenue, Ste B115
Bolling AFB, DC 20332-8050

10. SPONSORING/MONITORING AGENCY REPORT NUMBER
F49620-94-1-0008

11. SUPPLEMENTARY NOTES

19980615 041

12a. DISTRIBUTION AVAILABILITY STATEMENT
Approved for public release; distribution unlimited.

13. ABSTRACT *(Maximum 200 words)*

The recently emerging microelectromechanical technology has created a new frontier for the control of aerodynamic, structural and propulsion systems. The micromachining process provides two unique features for transducer technology: large in quantity and minute in size. A large number of sensors and actuators are essential for distributed system control while miniature transducers are necessary to satisfy high spatial resolution requirements. In this project, we suggest a microsystem concept which will make quantum advances to the still emerging microelectromechanical technology. The purpose is to develop a new conformable M^3 technology for use in active flow control on a delta wing. The M^3 technology will integrate microelectronics, microsensors, and microactuators on a planar silicon chip. The conformable M^3 technology has made another advancement to finish the integrated transducers and electronics on a flexible skin, hence called the smart skin here. To our knowledge, there is no existing technology and no ongoing research to provide conformable M^3 systems. In addition, potential applications of the smart skin in defense, aerospace and medical fields are obviously whenever 3-D surfaces are encountered. The smart skin is wrapped around the 3-D leading edge of a delta wing and controls all the six components of the aerodynamic forces and moments of a delta wing such that radical changes of aircraft design concept will take place.

14. SUBJECT TERMS

15. NUMBER OF PAGES
27

16. PRICE CODE

17. SECURITY CLASSIFICATION OF REPORT	18. SECURITY CLASSIFICATION OF THIS PAGE	19. SECURITY CLASSIFICATION OF ABSTRACT	20. LIMITATION OF ABSTRACT
Unclassified	Unclassified	Unclassified	UL

CONFORMABLE M^3 MICROSYSTEMS FOR AERODYNAMIC CONTROL

FINAL TECHNICAL REPORT

Air Force Grant No. F49620-94-1-0008

Chih-Ming Ho* and Yu-Chong Tai**

*Mechanical and Aerospace Engineering Department
University of California, Los Angeles
Los Angeles, California 90095

Phone: 310-825-2369 Fax: 310-206-2302
E-mail: chihming@seas.ucla.edu

** Division of Engineering and Applied Science
California Institute of Technology
Pasadena, California 91125

Phone: 818-395-8317 Fax: 818-584-9104
E-mail: yctai@touch.caltech.edu

CONTENTS

CHAPTER I : EXECUTIVE SUMMARY

1.1 Goal of Project

The purpose of this project is to demonstrate the feasibility of using micro actuators to control a macro aerodynamic device, like a delta wing, by manipulating boundary layer separation around the leading edge. Flow over a delta wing is characterized by a pair of symmetric primary vortices separated from the leading edge. At high angle of attack, these vortices contribute a great portion to total lift. Therefore, if we can use micro actuators to break the symmetry of vortices, it is possible to generate rolling moment, or even pitching and yawing moments by proper spatial actuation. The key point for this kind of flow control is the matching of length scale. If the size of the micro-actuator matches the thickness of the thin boundary layer near the leading edges of the delta wing, it is possible to use small actuation to perturb the flow and break the symmetry of the two leading edge separation vortices. This match provides a coupling between the micro actuator and the flow instability that serves as an effective amplifier of the artificial disturbances.

A novel flexible skin with integrated micro sensors, micro-actuators and logical decision electronics will be developed for accomplishing this challenging project.

1.2 Highlights of Accomplishments

In this report we have the following achievements:

Aerodynamic Tests:

- Maximum rolling, pitching, and yawing moment generated by 2 mm micro actuators for different angles of attack has been found. The optimum actuation locations for torque control have been also identified. These data are very important parameters for integrated M^3 system.

- A flexible skin with shear stress sensor arrays has been calibrated on a circular cylinder. The sensitivity of these sensors is consistent with one in turbulent 2-D channel flow. The separation point for flow over a circular cylinder is also confirmed by this setup.
- Extensive testing of a flexible skin with micro shear stress sensor arrays has been carried out. Flexible skin has been attached on a rounded leading edge to detect instantaneous separation line. Results show reasonable consistency exists when compared with one done by a single sensor.
- A new delta wing model with pressure taps on the surfaces to map out surface pressure distribution has been built. According to surface pressure data, the effect of actuation seems to move vortex structure inboard to generate negative rolling moment when actuators are located around the upper surface.
- New micro actuators with 1 mm size have been fabricated. With torsional bar, they can sustain wind tunnel testing up to 40 m/s. New micro actuators are also installed on the leading edge of a delta wing to investigate control authority. About 25 % change of rolling moment can be achieved by 1 mm actuation.
- A new Mirage III model airplane has been built during this reporting period. This airplane has a rounded leading edge on which miniature actuators are installed. Flight test shows that we can repeatedly achieve different maneuver pattern, including 180-degree turn.

Microfabrication Issues:

- We have successfully fabricated the first sensor and actuator array on a flexible skin.
- A process to fabricated a more robust flexible skin was developed, and a new run fabricating this skin was completed.
- In an effort to create more robust actuators that can be fabricated with a high yield, we have fabricated bulk micromachined actuators.
- As a first step towards complete integration, we have fabricated sensors, actuators, and electronics all on the same chip.

Control:

- A CMOS control circuit has been designed and sent to MOSIS for fabrication. It consists of two channels of CT bias circuits, gain stages, ac signal averaging circuits, comparator for these two channels and the driving circuit for an actuator.

1.3 Future Plan

In the next six months, we plan to focus on the following tasks:

(1) A PIV (Particle Image Velocimetry) system which enables us to map out velocity distribution on the suction side of a delta wing would be set up. We will investigate the interaction mechanism between micro actuators and large-scale primary vortices.

(2) Model airplane flight tests will be continued. A new micro actuator with stronger supporting device will be installed on the leading edge of model airplane to explore the feasibility of using M^3 system to control a macro aerodynamic devices.

(3) After the chip from MOSIS is fabricated, it will be tested to confirm that it works as designed.

(4) The process and layout design for the integration of the shear stress sensors, micro-actuators and the control circuit on a flexible skin will be conducted. The layout will be sent to Orbit for the fabrication of the CMOS circuit. The fabrication of sensors and actuators will be performed on the wafers back from Orbit in Caltech Micromachining Laboratory.

CHAPTER II: FACILITIES AND INSTRUMENTATION

Brief summary of facilities and instrumentation will be presented here. Details of the set-up can be found in the previous progress reports.

2.1 Wind Tunnel

An open-return wind tunnel has been set up at UCLA for aerodynamic tests. The test-section is 3 ft x 3 ft and 22 ft long. The maximum operating speed of this wind tunnel is 45 m/s. The turbulence level of the wind tunnel is about 0.6 %.

2.2 Wing Model

A delta wing model with a swept angle of 56.5° was employed for this study. The delta wing model has rounded leading edges which enables us to manipulate separation region. Since the limited supply of micro actuators, both micromachined actuators and mechanical actuators were used for this study.

Micromachined actuators and micro shear stress sensors were placed on a cylindrical rod located at the leading edges of a delta wing. The rod can be rotated such that the positions of these transducers can be changed to cover the leading edge area.

Strip-type mechanical actuators were installed inside thin slots. The actuators can be extended 1 or 2 mm out of plane. The location of the actuators can be controlled by rotating the leading edge rod.

2.3. Instrumentation

A six component force/moment transducer (AMTI, INC.) was used to measure aerodynamic forces and moments. During the past reporting period, this six component force/moment transducer has been fully calibrated.

CHAPTER III: AERODYNAMIC TESTS

3.1 Status Overview

Maximum rolling, pitching, and yawing moment generated by 2 mm micro actuators for different angles of attack has been found during this reporting period. The optimum actuation locations for torque control have also been identified. With this information, we can better understand the control authority of micro actuators.

A flexible skin with shear stress sensor arrays has been calibrated on a circular cylinder. The separation point for laminar flow over a circular cylinder is also confirmed by this setup. Extensive testing of a flexible skin have been conducted. The flexible skin has been attached on a rounded leading edge to detect instantaneous separation line. Results show reasonable consistency exists in comparison with one done by a single sensor.

A new delta wing model with pressure taps on the has been built surfaces to map out surface pressure distribution. According to surface pressure data, the effect of actuation seems to move vortex structure inboard to generate negative rolling moment when actuators are located around the upper surface.

New micro actuators with 1 mm size have been fabricated. New micro actuators were installed on the leading edge of a delta wing to investigate control authority. About 25 % change of rolling moment can be achieved by 1 mm actuation.

A new Mirage III model airplane has been built during this reporting period. This airplane has a rounded leading edge on which miniature actuators are installed. Flight test shows that we can repeatedly achieve different maneuver pattern, including 180-degree turn.

3.2 Maximum Rolling, Pitching, Yawing Moments for Different AOA

A delta wing with a swept angle of 56.5° was mounted on a six-component force/moment transducer which records forces and moments in all three axes. An

actuator extends from the apex to the trailing edge; this A-T actuator was installed to alter the separation zone in order to control the moments. The location of the actuator is indicated by the angle, θ, which is measured from the lower surface of the wing (Fig. 3.2.1). For angle of attack ranging from 3° to 35°, the incremental torque generated by the actuation, M_r, was normalized by the torque produced by the vortex lift, M_v, which is the product of the lift generated by a singe leading edge vortex and the distance between the centroid of half wing and the center line. In this report, M_v at, $\alpha = 30°$ was used for all the normalization.

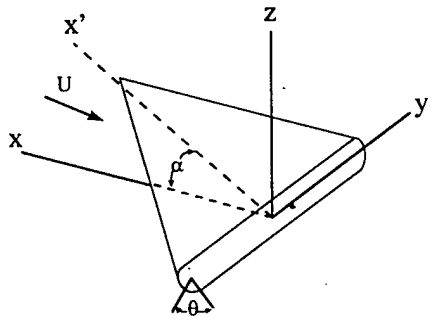

Fig. 3.2.1 Schematic representation of delta wing system

We use two-sided actuation to find out maximum level of moment control at different AOA. Figures 3.2.2 - 3.2.4 show that maximum rolling moment is obtained at $\alpha = 25°$ and about 70 % change of rolling moment can be achieved. However, only about 20 % change of rolling moment is observed for low AOA. For pitching moment, we have maximum control ability at $\alpha = 35°$. About 50 - 60 % change of pitching moment can be generated by 2 mm actuation. In addition that we find high pitching moment at high AOA, it is surprising that very large pitching moment also takes place at low AOA, like 3° - 6°. The pattern for yawing moment is very different from that of rolling and pitching moment. Only 10 % change of yawing moment can be found at large AOA. Nonetheless, we did find very large yawing moment (about 20 %) at low AOA.

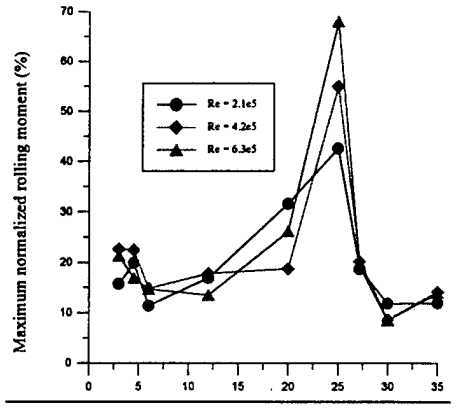

Fig. 3.2.2 Maximum normalized rolling moment for different AOA

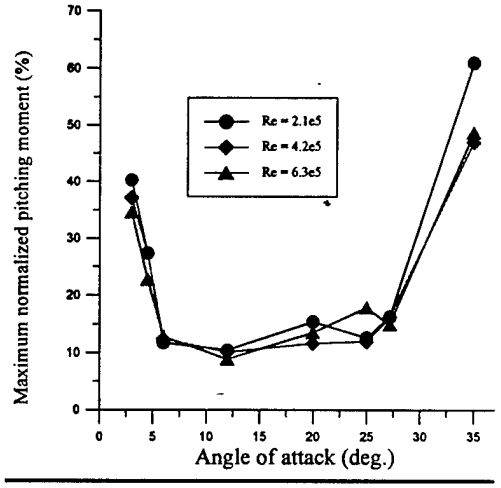

Fig. 3.2.3 Maximum normalized pitching moment for different AOA

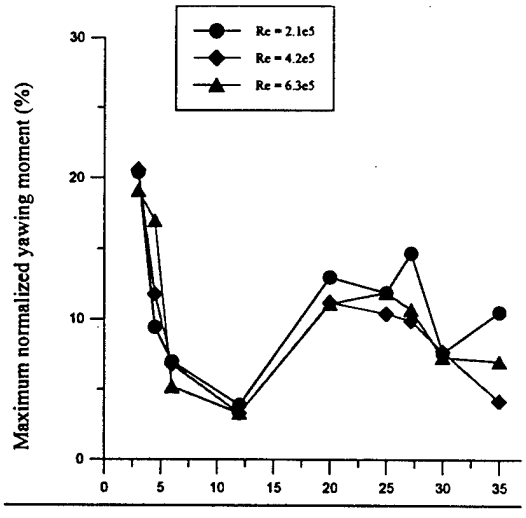

Fig. 3.2.4 Maximum normalized yawing moment for different AOA

3.3 Calibration of Flexible Skin on a Circular Cylinder

In this report, a flexible skin with shear stress sensor arrays has been developed and calibrated for flow over a circular cylinder. Fig. 3.3.1 shows a picture of the 1cm x 3.2 cm skin. It has two columns of 32 shear stress sensors each and can cover the 1 cm wide portion of the leading edge completely. The flexible skin is attached to circular cylinder (Fig. 3.3.2) to calibrate its sensitivity. Fig. 3.3.3 shows the calibration results using a constant temperature circuit with an overheat ratio of 10 %. The data shows a linear relation between V^2 and $\tau^{1/3}$, where V is the first stage voltage output and τ is the wall shear stress. In Fig. 3.3.3, calibration data for flexible skin in 2-D channel flow are also presented for comparison. Very reasonable consistency exists when we compare their slope. For hot-film sensors, output of sensors depends on local heat transfer. Two major parameters can affect convective heat transfer: surface shear stress and local pressure gradient [1]. Flow over a circular cylinder has varied pressure gradient due to local curvature. However, flow in 2-D channel has constant pressure gradient determined by upstream condition. From the result in Fig. 3.3.3, it means that surface shear stress term is dominant in both flow conditions. Detailed calculation also shows the same results.

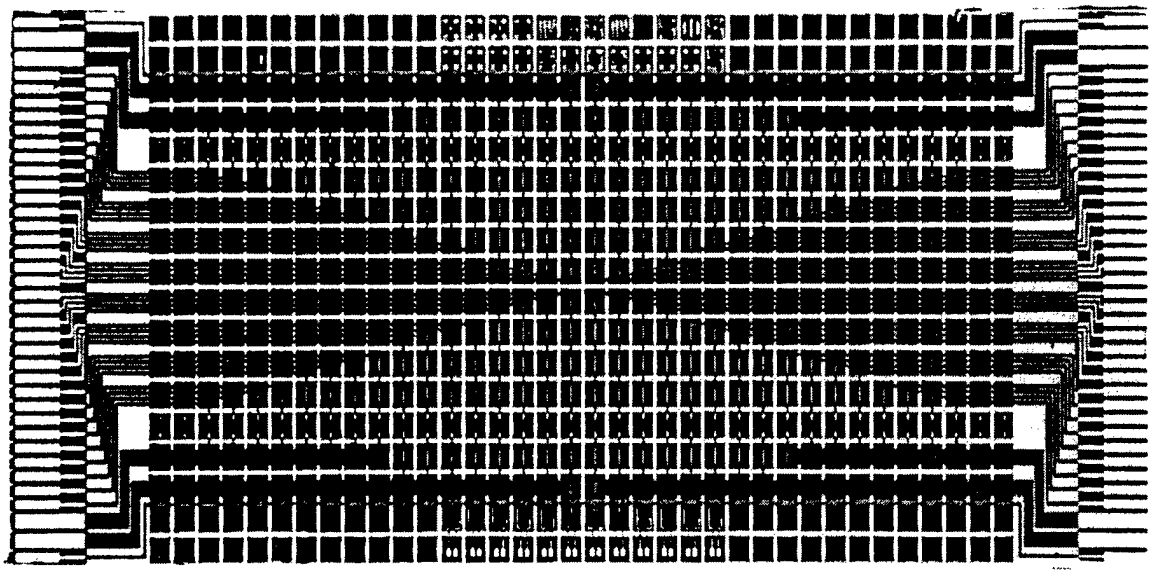

Fig. 3.3.1 Flexible skin with shear stress sensor array

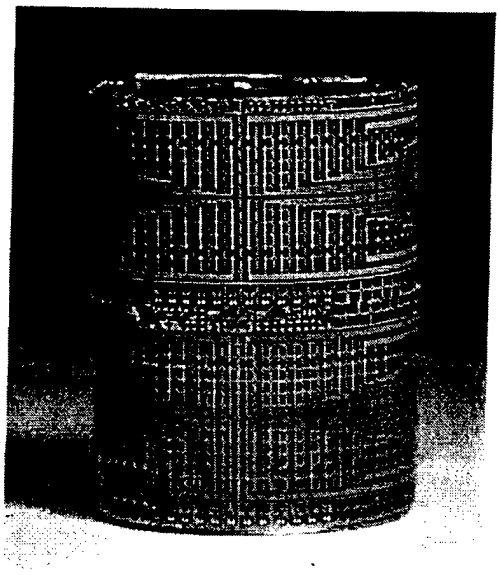

Fig. 3.3.2 Flexible skin on a circular cylinder

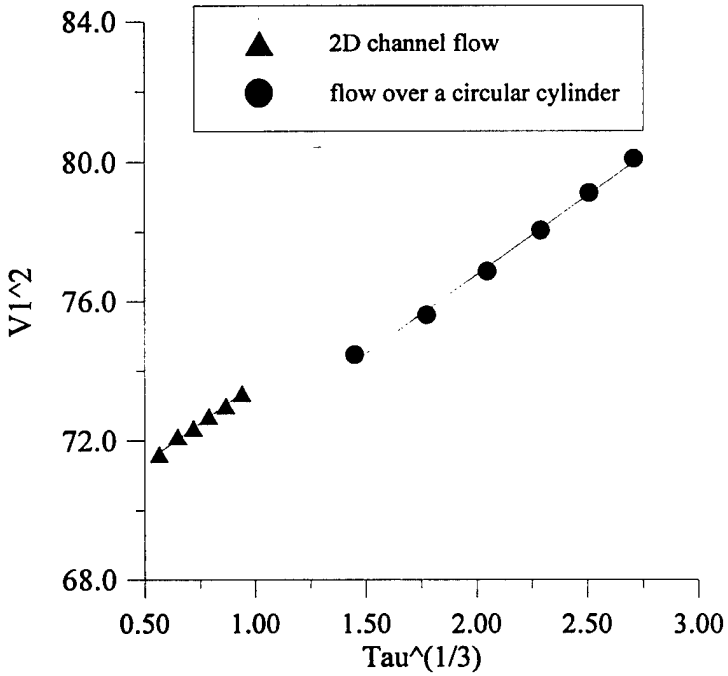

Fig. 3.3.3 Calibration data of flexible skin in different flow conditions

When we calibrated our flexible skin on a circular cylinder, we also successfully detect separation point. The position of separation point for flow over a circular cylinder has been investigated in the literature. For flow with Reynolds number

lower than $2x10^5$, it is laminar flow and its corresponding position for separation point is at about 80° measured from stagnation point [2]. Bellhouse [3] used single hot-film sensor to detect separation point in 1966 and he reported that DC signal reaches a local minimum at separation and a sudden jump of RMS signal occurs. Our measurement shows the same trend. Figure 3.3.4 indicates that separation point is located near 80°, where a minimum value of DC output take places. An abrupt increase in RMS signal shown in Fig. 3.3.5 also supports our point.

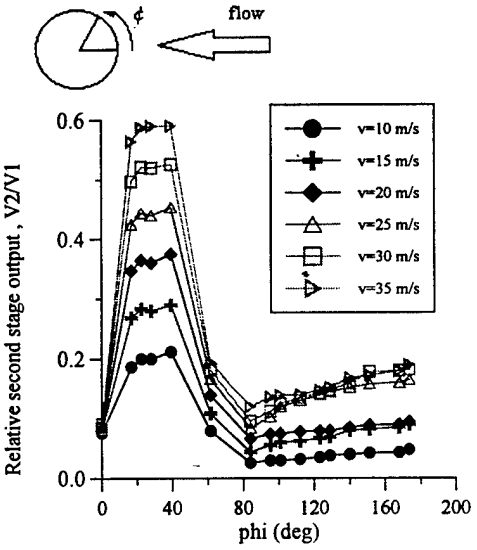

Fig. 3.3.4 DC output from flexible skin at different velocities

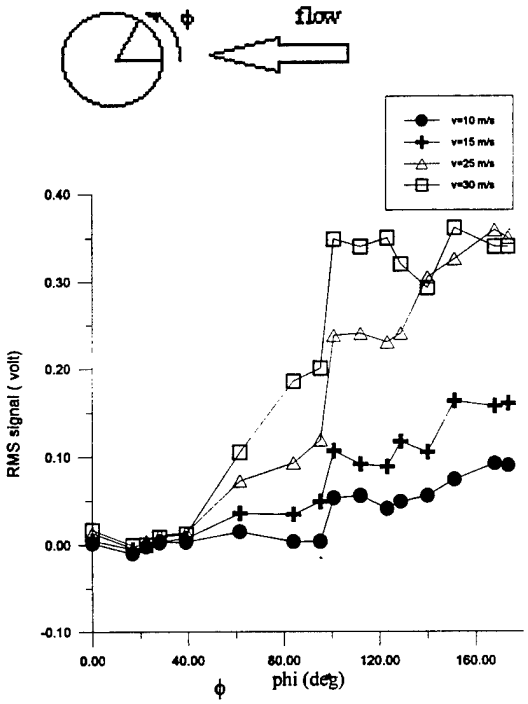

Fig. 3.3.5 RMS signal from flexible skin at different velocities

3.4 Separation Line Detected by _Flexible Skin

In the past reporting periods, we successfully detected the separation line by using a single sensor located on leading edge rod. By rotating this rod, we can map out the shear stress distribution on the leading edge and determine the location of separation line. However, we cannot detect instantaneous separation line by this setup. During dynamic maneuver, we expect separation line would change with local flow condition and some devices which can wrap around the curved surface with enough sensing elements are necessary for this project.

A flexible skin with shear stress arrays has been fabricated and calibrated on a circular cylinder. After calibration, we put the flexible skin on the leading edge of a delta wing and try to detect separation line instantaneously. Figure 3.4.1 shows the results obtained by flexible skin at AOA=30°, L= 28 cm (where L is the distance measured from the apex) while compared with that by a single sensor. Very good agreement has been observed in this figure. In order to detect separation line along the leading edge, we attached flexible skin on a small piece of circular cylinder with 2 cm length and move

this small piece from apex to trailing edge. Figures 3.4.2 (a) - (b) indicate the correlation between separation line and optimum location for roll control obtained by micro actuator testing. It shows that we have to perturb the flow right ahead of separation line in order to interact with thin boundary layer before separation. Results also suggest that distributed control of actuators is necessary since separation line is a curved line.

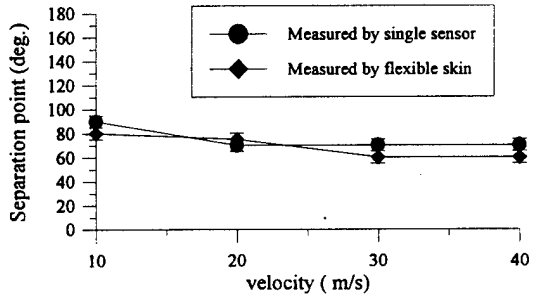

Fig. 3.4.1 Comparison of the results between flexible skin and a single sensor

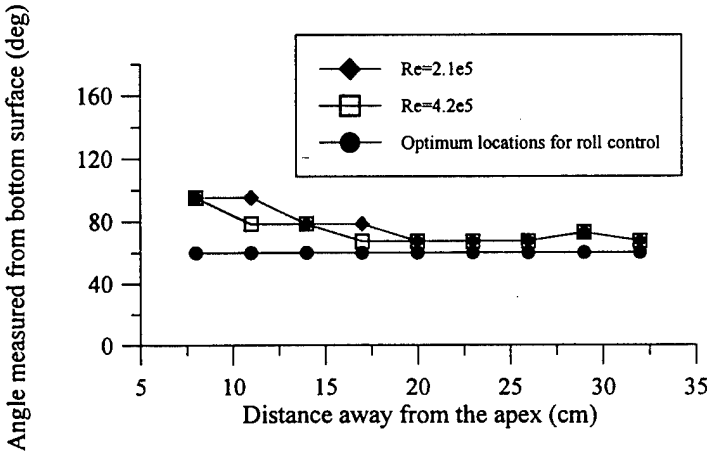

Fig. 3.4.2(a) Separation line vs. optimum location for roll control at AOA=25°, low Reynolds number

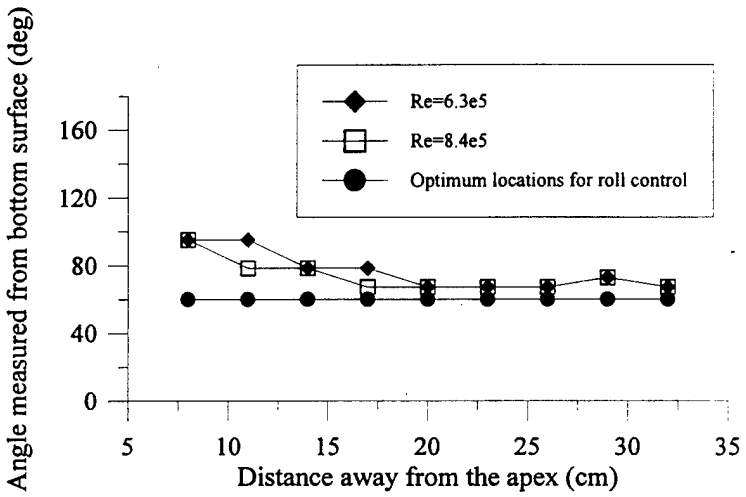

Fig. 3.4.2(b) Separation line vs. optimum location for roll control at AOA=25°, high Reynolds number

3.5 Surface Pressure Measurement

Flow separating from delta wings along with each leading edge will form free shear layers. The shear layer rolls up into a core of high vorticity lying above the leeward side of the wing. The axisymmetric vortex core grows in radius in the downstream direction and transverse size is in the order of the half span. Each of the two leading edge vortices contains axial flow components in the central core region, and corresponding form a low pressure region. The pressure measurements by Fink and Taylor [4] showed that the location of maximum suction are beneath the core vortices (Fig. 3.5.1). As the core vorticity and axial speeds increase in the downstream direction, continuous drop in the core pressure is observed until vortex breakdown occurs.

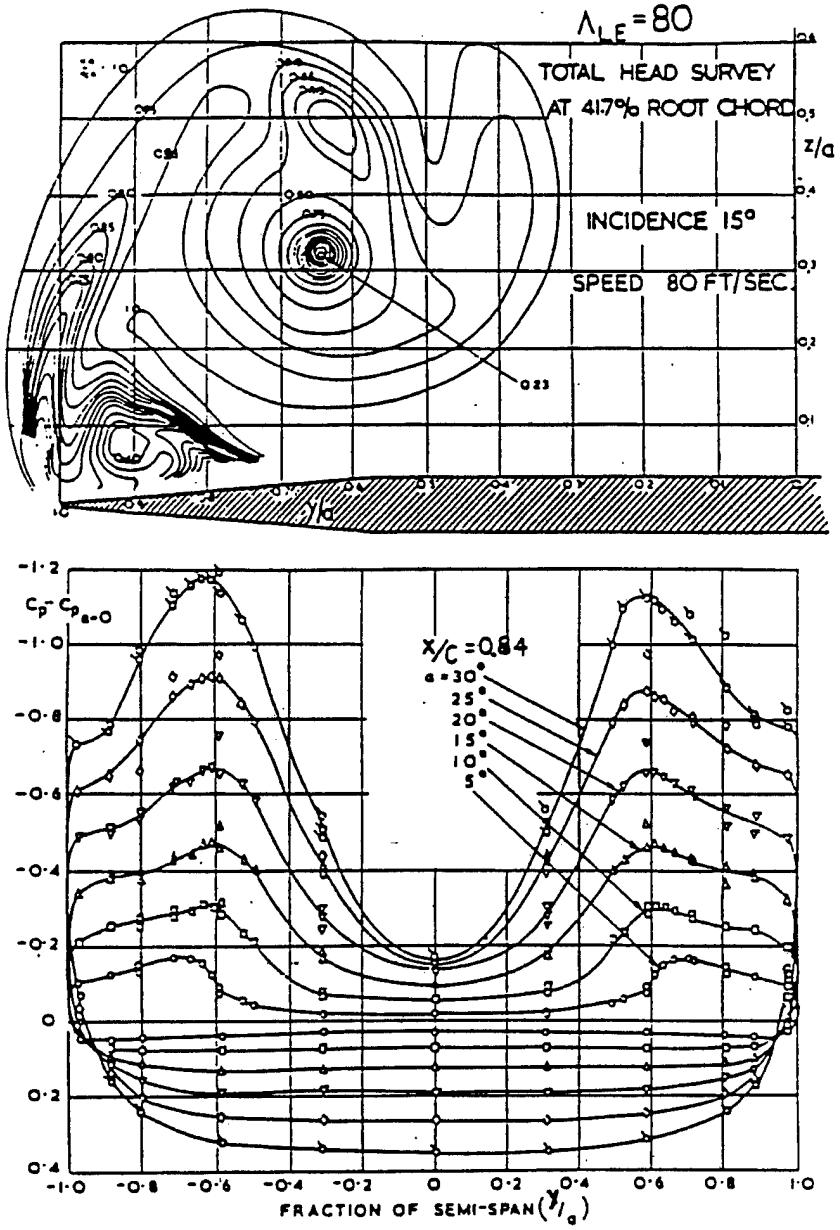

Fig. 3.5.1 Surface pressure measurements , Fink and Taylor [1967]

In order to better understand the interaction between micro actuators and leading edge vortices, we conducted an experiment measuring surface pressure distribution on the upper side of a delta wing. A new delta wing model with pressure tapes on the surface has been built during this reporting period. Figure 3.5.2 shows schematic representation of

wing model. Due to the limit of our current setup, only 7 cross-section data can be obtained. At each cross section, we have 12 measuring point in half span.

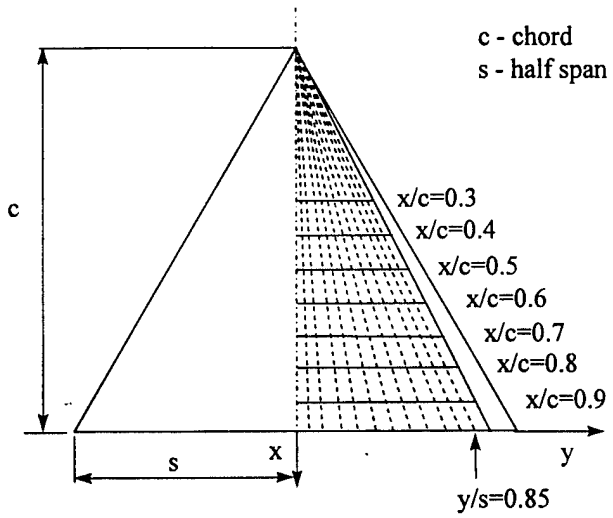

Fig. 3.5.2 schematic setup for surface pressure measurement for a delta wing

A commercial solid state gauge pressure sensor (NPC-1210, Lucas NovaSensor) has been used for this study. The full scale range is 5 psi. With constant-current circuit and 2nd stage amplifier, the sensitivity of the sensor has been calibrated as 8 volts/ psi. over our operating range (Fig. 3.5.3). After we finished calibrating the pressure sensor, we can map out pressure distribution on the upper surface and investigate the effect of micro actuators on the surface pressure. Figure 3.5.4 represents the variation of pressure coefficient, C_p, along spanwise location for different cross section. A peak of negative pressure coefficient appears in each case. It indicates that a well defined vortex structure is formed and vortex core is located at this position. As we activate the actuation, surface pressure distribution changes (Fig. 3.5.5). According to preliminary data, the effect of actuation seems to move vortex structure inboard to generate negative rolling moment when actuators are located around the upper surface.

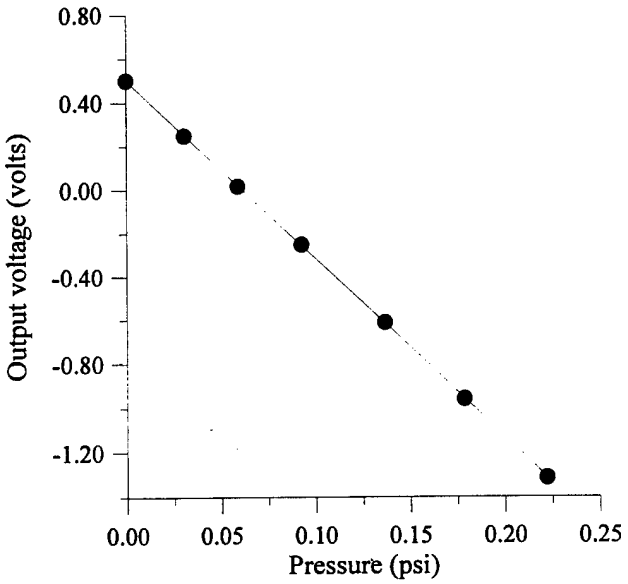

Fig. 3.5.3 Calibration of pressure sensor, NPC-1210

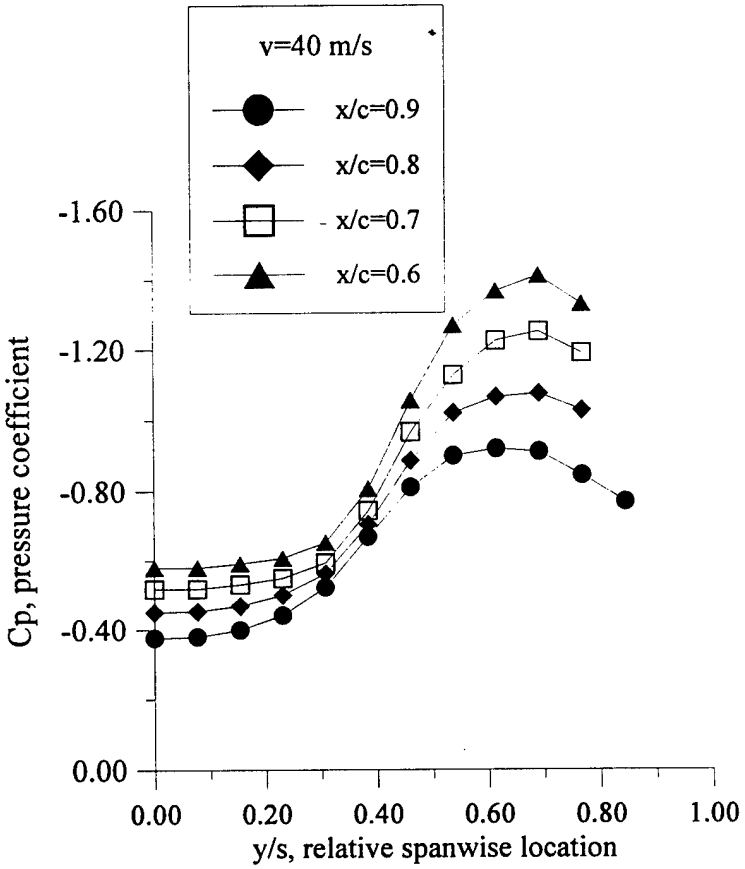

Fig. 3.5.4 Pressure coefficient variation along spanwise direction

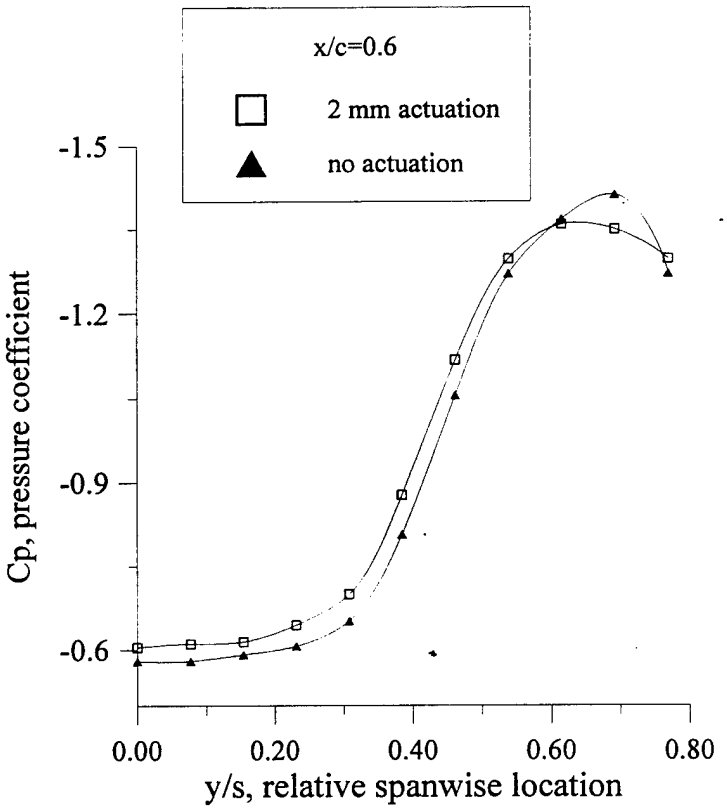

Fig.3.5.4 Pressure coefficient variation without actuation along spanwise direction in comparison with case with 2 mm actuation

3.6 New Micro Actuator Testing

New micro actuators with 1 mm x 1mm dimensions have been fabricated (Fig. 3.6.1) in this reporting period. With torsional bar of 500 x 30 μm^2, they can sustain wind tunnel testing up to 40 m/s. New micro actuators are also installed on the leading edges of a delta wing to investigate control authority. Figure 3.6.2 shows the effect of 1 mm actuators on the aerodynamics of a delta wing in terms of change of rolling moment at angle of attack of 25°. About 10 % change of rolling moment can be generated at $\theta = 60°$ for all Reynolds number. We also get -15 % at $\theta = 80°$ for large Reynolds number. If we employ two-sided actuation we mentioned in previous report, we could get about 25 % change of rolling moment by 1 mm actuation.

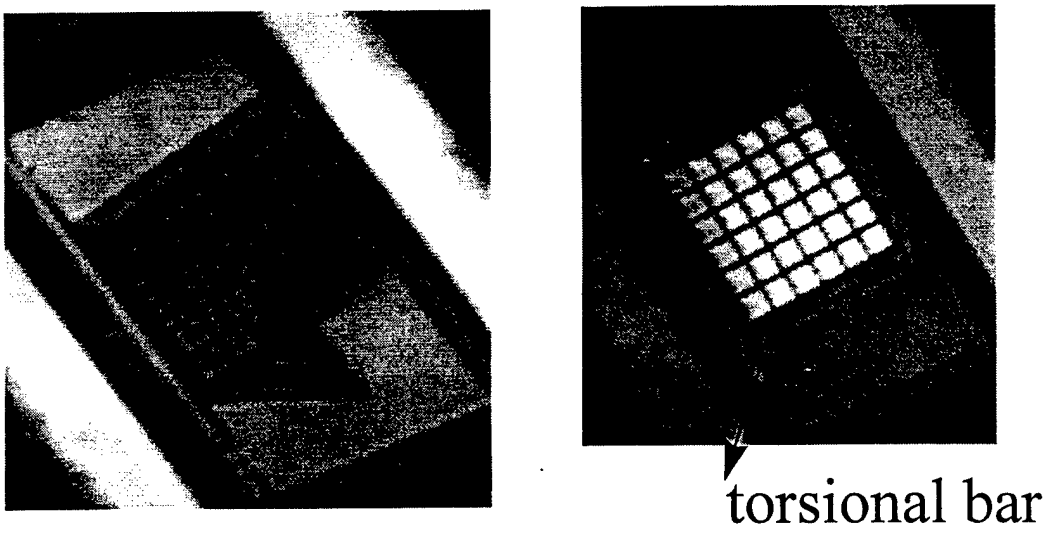

Fig. 3.6.1 Pictures of micro actuator

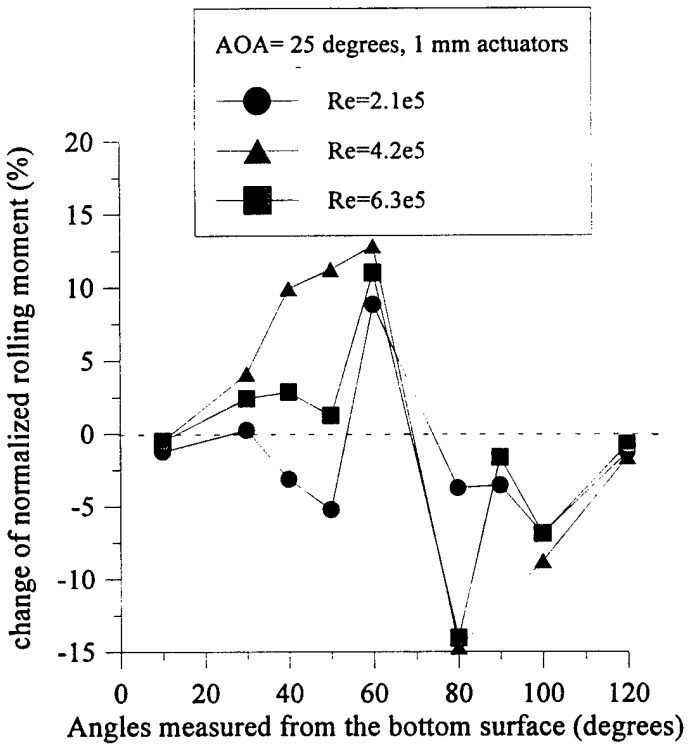

Fig. 3.6.2 Normalized rolling moment vs. actuation location, 1mm actuator

CHAPTER IV : DEVELOPMENTS OF MICRO MAGNETIC ACTUATORS AND FLEXIBLE SKIN

4.1 Status Overview

We have designed and fabricated permalloy actuators of different geometries for UCLA's wind tunnel tests. We have also investigated using bulk micromaching to create extremely robust actuators which can be processed with a high yield.

We have also designed and fabricated more robust flexible skin with arrays of shear stress sensors by the polyimide coating on the backside of the skin.

We have designed and fabricated a flexible skin with arrays of shear stress sensors and surface micromachined magnetic coil actuators.

We have designed the CMOS CT bias circuit and the basic control circuit to identify the separation point from the outputs of shear stress sensors and drive the corresponding actuators. The layout has been sent to MOSIS for fabrication.

Finally, we have designed and fabricated an integrated chip containing sensors, actuators and electronics on the same substrate.

4.2 Bulk Actuator

We have done extensive testing using permalloy surface micromachined actuators. However, one inherent problem in surface micromachining is stiction. Traditionally, a wet release agent is used to free the structural layer. After the release, the surface tension of the etchant often pulls the structural layer down to the substrate, and a

permanent bond is often formed. A bulk micromachined actuator (Fig. 4.2.1) has no such problem, however, because there is no layer lying underneath the flap. In addition, the structural layer is single crystal silicon and can be tens of microns thick, making it much more robust than a surface micromachined actuator.

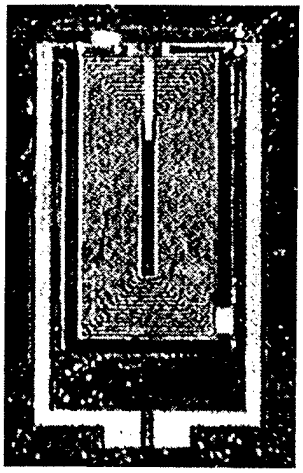

Fig 4.2.1. A bulk micromachined flap. The flap is 2.5x1 mm^2.

4.3 Flexible Skin

The flexible skin we developed previously has 7 μm polyimide layers only on the front side of the skin. The maximum tensile force of the 3 x 1 cm2 skin is about 14.7 kg along its longitudinal direction. However, the peel-off forces of the polyimide from Si substrates given by the manufacturer is only about 0.23 g/mm, or 2.3 g for our skin.. Therefore, even a very small shear force exerted on a Si island would peel it off. The solution to this problem is to spin thick polyimide (10 μm) on the back side of the wafer to fully encapsulate the islands. This also increases the maximum tensile force the skin can stand to 35.7 kg.

We have successfully fabricated sensor and actuator skin using the process presented in the previous progress report. The following are the pictures of the skin. However, the robustness of the actuators needs to be improved.

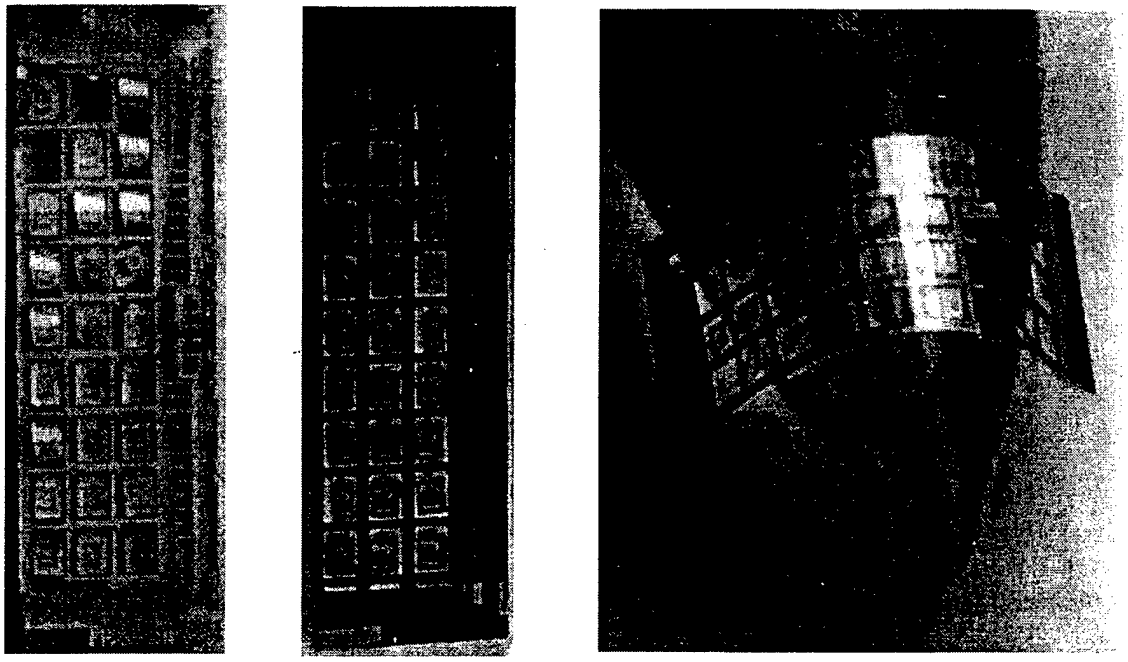

Front side Back side Sitting on a conic object

Fig. 4.3.1 Pictures of the sensor and actuator skin.

4.4 Shear stress sensors for CMOS integration

The shear stress sensors built on the previous skins has a polysilicon wire 150 μm long and 3 μm wide. It needs about 3 volts to operate at an over-heat ratio of 0.1. When it operates in constant temperature mode, the overall voltage drop on the wheatstone bridge is above 5.5 volts, the upper limit of the power supply for general CMOS circuits. Therefore, we have to lower the sensor voltage to under 2 volts in order to integrate it with CMOS circuits.

We have noticed that the power consumption of a sensor does not increase significantly as the width of the polysilicon wire increase, while the sensor resistance is

inversely proportional to the width. Therefore the sensor voltage is approximately inversely proportional to the square root of the width. By increase the width from 3 μm to 11 μm or above, we are able to lower the sensor voltage to under 2 volts. Fig. 4.4.1 shows the picture of a 15 μm wide sensor. Also, the wind-tunnel testing results in Fig. 4.4.2 has shown that the relative sensitivity for sensors with different widths are nearly the same.

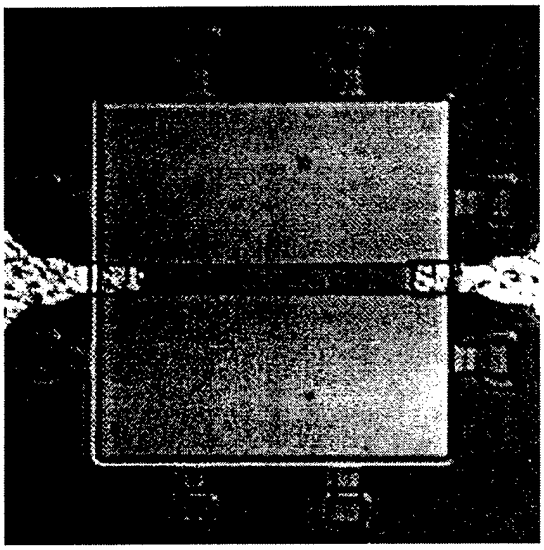

Fig. 4.4.1 Picture of a shear stress sensor with 15 μm wire 150 μm long polysilicon wire.

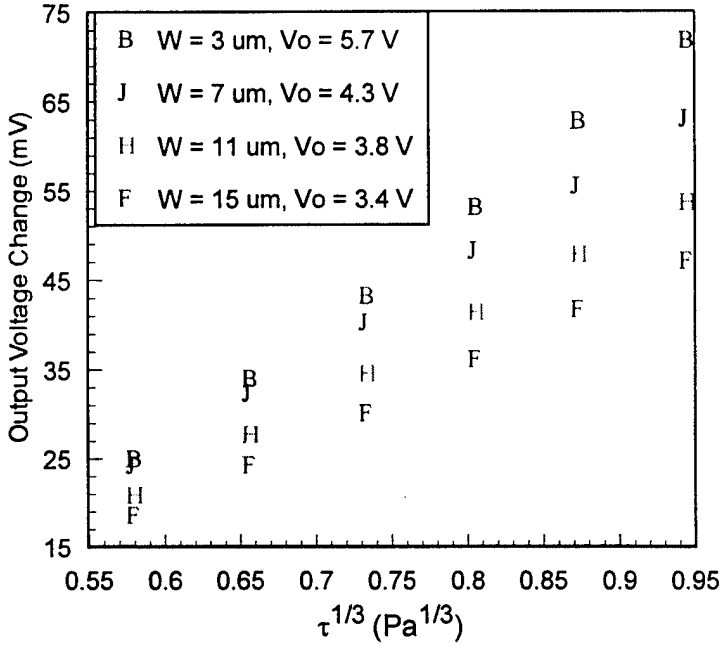

Fig. 4.4.2 Calibration results of sensors with different widths.

4.5 CMOS Control Circuit

The circuit consists of two channels of CT bias and ac gain stages. The signal from the ac gain stage is then fed to a leaky integrator. The leaky integrator integrates the absolute value of the input signal with a leaky path and its output signal is proportional to the RMS of the input signal. The outputs from these two integrators are compared through a bump circuit. If one output is significantly larger than the other (say twice larger), then the bump circuit outputs a signal indicating that there exists a flow separation between these two sensors. Finally, this signal is amplified on the output stages to drive the proper actuators. Figs. 4.5.1 and 4.5.2 are the block diagram and the CMOS layout of this circuit respectively. The layout has been sent to MOSIS and is currently in fabrication. The fabricated circuit will be tested with external sensors and actuators to confirm that they perform the desired functions. If it works, it will be integrated with sensors and actuators on a flexible skin to complete the M^3 system.

Fig. 4.5.1 Block diagram of the control circuit

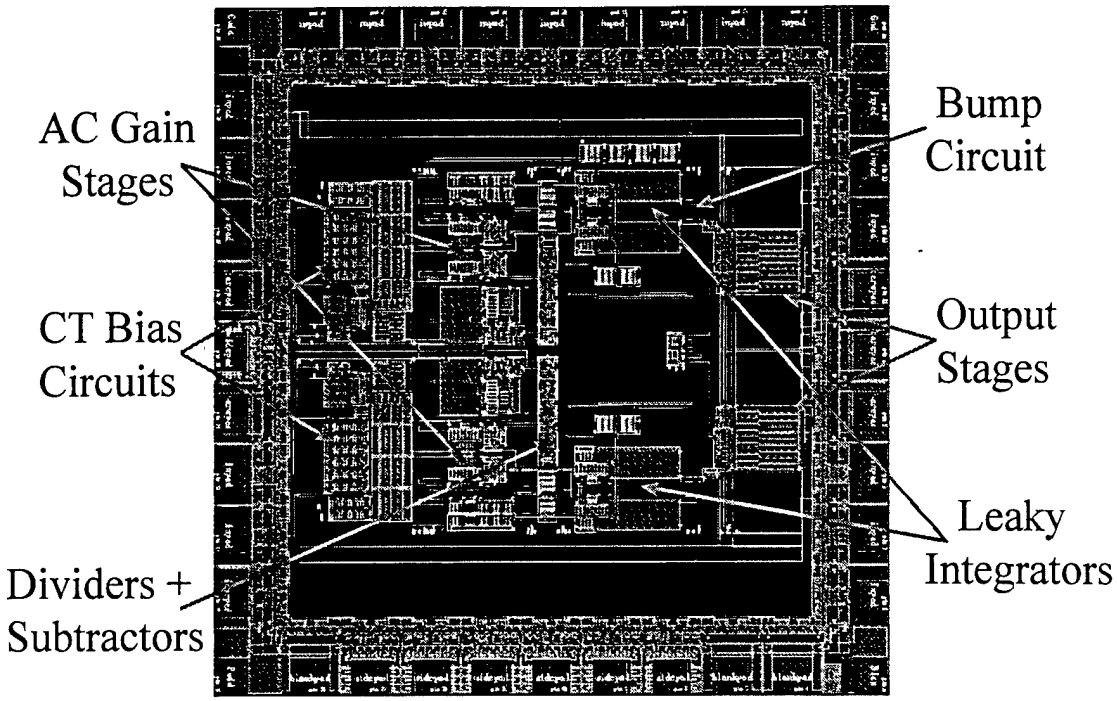

Fig. 4.5.2 Design layout of the control circuit

4.6 Sensor, Actuator, Electronic Integration

One final goal of the project is to fabricate sensors, actuators, and electronics on a flexible skin. One base step that must be accomplished before such a formidable task can be undertaken is to fabricate sensors, actuators, and electronics on a rigid wafer. We have fabricated this. Fig 4.6.1 shows one die from the run.

The fabrication is done both at CalTech and at the University of California - Berkeley. We first send the wafers to Berkeley's microlab for initial CMOS circuitry fabrication up to, but not including, contact hole openings for metallization. We then do the initial sensor and actuator fabrication, completing all of the high temperature steps. The wafers then go back to Berkeley where contact holes are opened, and circuit metallization is done. We then take the wafers and complete the sensor and actuator fabrication, concluding with the release of the actuator.

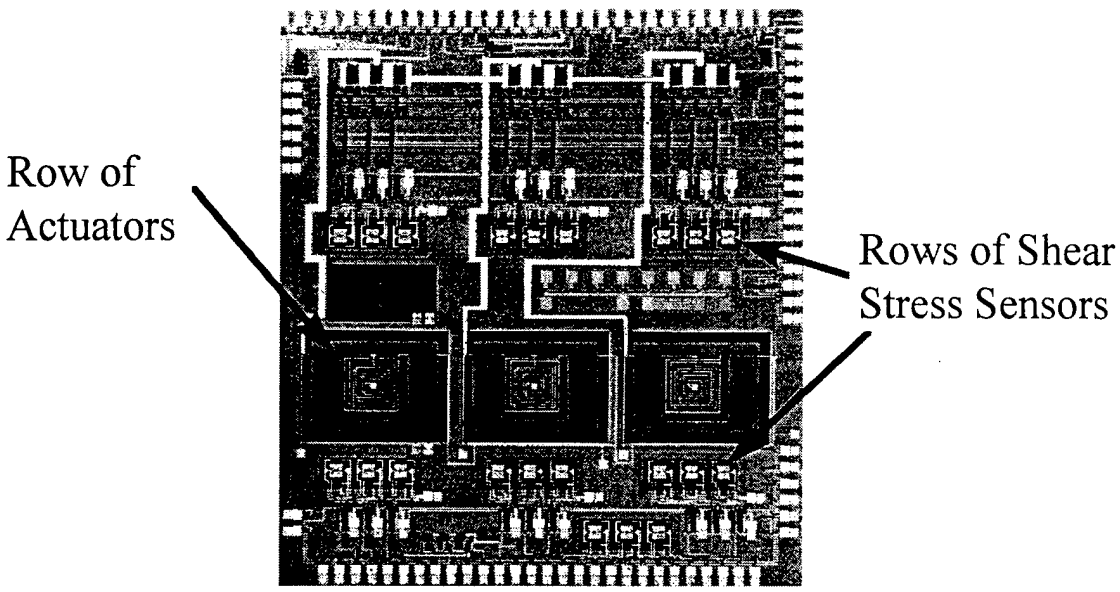

Fig 4.6.1 A die with integrated sensors, actuators and electronics. The die size is 1 cm^2. Polysilicon was used as the sacrificial layer for the actuators, which were released using BrF_3 gas, a dry release method.

This process requires approximately 35 masking steps and is much more complicated than the sum of the individual processes. Many steps are included as protection steps - ensuring that one part of the wafer is unaffected while another part is being processed. In addition, many other steps are added to help improve the robustness of the process, in essence making the process more conservative.

This fabrication run included surface micromachined actuators. We chose polysilicon instead of oxide for the sacrificial layer. The two reasons for this choice are both related to the sacrificial layer etch. When using oxide, hydrofluoric acid (HF) is used as the release agent. HF attacks aluminum, which is used as circuit metallization. In addition, oxide is used as a protection layer for the circuitry fabrication and would therefore be destroyed by the HF release etch.

In using polysilicon as the sacrificial layer, we experimented with both wet and dry release techniques. We developed a novel technique using BrF_3 gas for dry release. This was developed in hopes of solving the stiction problem associated with wet releases.

One problem with using BrF_3, however, is that is attacks silicon nitride at an appreciable rate. One solution is to use a combination of wet and dry release techniques.

References

1. Spence D. A. and Brown G. L., "Heat transfer to a quadratic shear profile", Journal of Fluid Mechanics, vol. 33, 1968, pp. 753-773.

2. White, F. M., *Fluid Mechanics*, 3rd ed., McGraw Hill, New York, 1994, pp.413 - 422.

3. Bellhouse, B. J. and Schultz D. L., " Determination of mean and dynamic skin friction, separation and transition in low-speed flow with a thin-film heated element ", Journal of Fluid Mechanics, vol. 24, part 2, pp. 379 - 400, 1966.